Journal of The Electrochemical Society, **161** (10) D528-D533 (2014)
0013-4651/2014/161(10)/D528/6/$31.00 © The Electrochemical Society

Influences of Cerium on the Electrodeposition Process and Physicochemical Properties of Lead Dioxide Electrodes

Yingwu Yao,[a,z] Lihua Cui,[a] Chunmei Zhao,[b,z] and Limiao Jiao[a]

[a]*Hebei University of Technology, School of Chemical Engineering and Technology, Electrochemical Surface Technology Research Laboratory, Tianjin 300130, People's Republic of China*
[b]*Hebei University of Technology, School of Architecture & Art Design, Tianjin 300401, People's Republic of China*

The influence of cerium on lead dioxide electrodeposition process on a glass carbon electrode (GCE) from lead nitrate solution was studied by cyclic voltammetry (CV), chronoamperometry (CA) and electrochemical impedance spectroscopy (EIS). Cerium exhibit an inhibition effect on the lead dioxide electrodeposition process. Instantaneous nucleation mechanism can be found for lead dioxide electrodeposition according to Scharifker–Hills' model with three-dimensional growth, which is not influenced by the addition of cerium. The morphology and structure of Ce-doped PbO_2 electrodes were investigated by scanning electron microscopy (SEM) and X-ray diffraction (XRD). The results show that the adulteration of cerium can greatly decrease grain size and make the films more compact. Accelerated lifetime tests demonstrate that the adulteration of cerium can highly lengthen the service life of Ce-doped PbO_2 electrode in its practical application. Methylene blue degradation experiments reveal that the Ce-doped PbO_2 electrodes possess excellent electrocatalytic activity.

Manuscript submitted May 28, 2014; revised manuscript received July 11, 2014. Published July 23, 2014.

PbO_2 has been regarded as an excellent metal oxide electrode because of its lower price, good chemical stability and high oxygen evolution overpotential.[1,2] Today, PbO_2 electrodes have been used in many industry fields, such as batteries,[3] wastewater treatment,[4–7] electrosynthesis,[8] ozone generation[9] and analytical sensors.[10]

The electrochemical properties of PbO_2 electrodes are strongly affected by the incorporation of some foreign ions or particles, such as Bi,[11] F,[12] Co_3O_4,[13] TiO_2[14–16] and ZrO_2,[17] which can considerably strengthen the electrocatalytic activity and stability of PbO_2 electrodes. These studies indicate that the properties of PbO_2 electrodes, such as morphology, structure and electrochemical degradation ability, are influenced significantly by doping with metal ions or oxides.

Cerium is an attractive rare earth element with high thermal stability, electrical conductivity and diffusivity.[18] With its ability to switch between +3 and +4 oxidation states under oxidization or reduction processes and the facile formation of labile oxygen vacancies that function catalytically with anodic oxygen transfer reaction, cerium is considered as a powerful oxidant that can readily oxidize organic pollutants.[19,20] The use of cerium as a catalyst in oxidation reactions shows that cerium is a promising dopant to improve the electrocatalytic activity of PbO_2 electrodes.[21] Recently, cerium has been doped into PbO_2 electrodes to enhance their electrocatalytic capacities.[22,23]

In this paper, the Ce-doped PbO_2 electrodes were prepared with different cerium content. The influence of cerium on lead dioxide electrodeposition process in lead nitrate solution was investigated by cyclic voltammetry (CV), chronoamperometry (CA) and electrochemical impedance spectroscopy (EIS). Scanning electron microscope (SEM) and X-ray diffraction (XRD) were used to examine the morphology and structure of Ce-doped PbO_2 electrodes. Service life of Ce-doped PbO_2 electrodes was evaluated by accelerate life test. The oxygen evolution overpotential of Ce-doped PbO_2 electrodes was tested by the linear polarization curves. Methylene blue (MB) was chosen as model pollutants to evaluate the effects of cerium on the electrocatalytic activity of Ce-doped PbO_2 electrodes.

Experimental

Electrodeposition process.— Electrochemical measurements were performed at CHI660D electrochemical workstation (CH Instruments, Shanghai, China). A glassy carbon electrode (GCE) with a diameter of 3 mm was used as the working electrode, platinum electrode as the counter electrode (CE), and a saturated calomel electrode (SCE) as the reference electrode (RE). The GCE was carefully polished with successively finer grades of aluminum slurry (10, 3.5, 1.5, 0.3 and 0.05 μm, respectively), and then cleaned ultrasonically in distilled water to remove any residues from the polishing process. It was rinsed with distilled water prior to each experiment.

Cyclic voltammetry was carried out with scanning rate of 50 mV s^{-1}. The current transients obtained from chronoamperometry experiments were performed with single positive potential steps from the open-circuit potential. The electrochemical impedance spectroscopy was measured at 1.7 V (vs. SCE), and the measurement frequency range was set from 100,000 to 0.01 Hz. Without special mention, all the electrochemical experiments were carried out at ambient temperature. Solution was unstirred during the experiment process.

Preparation and characterization of Ce-doped PbO_2 electrodes.— *Preparation of Ti/SnO_2-Sb_2O_3 interlayer.*— Ti plates (99.5%, 20 mm × 50 mm) were degreased in absolute ethanol for 20 min, then polished by 320-grit paper, and the plates were cleaned by ultrasound for 10 min. Next, Ti plates were treated in boiling aqueous 20% oxalic acid for 2 h, followed by thorough washing with de-ionized, doubly distilled water. The SnO_2-Sb_2O_3 interlayer deposited on the Ti plates was prepared by thermal decomposition. 20.0 g $SnCl_2$, 2.0 g $SbCl_3$ and 13.2 mL concentrated HCl were dissolved in 100 mL isopropanol. The Ti plates were dipped in the solution for 5 min, then dried at 100°C for 15 min, and the same procedure was repeated four times. Then, the Ti plates were thermally treated in a muffle furnace at 500°C for 2 h.

Preparation of Ce-doped PbO_2 electrodes.—The Ce-doped PbO_2 electrodes were prepared by anodic electrodeposition method. The composition of the plating bath was: 0.2 mol L^{-1} $Pb(NO_3)_2$, 0.1 mol L^{-1} HNO_3 and different concentrations of $Ce(NO_3)_3$ (1, 2 and 3 mmol L^{-1}). The Pb electrode was used as the cathode, the anode was Ti coated with a SnO_2-Sb_2O_3 interlayer. The electrodeposition conditions were current density 30 mA cm^{-2} and bath temperature 30°C, based on our previous study.[17] These electrodes prepared under same conditions with different concentrations of cerium ions are labeled as Ce-PbO_2(1), Ce-PbO_2(2) and Ce-PbO_2(3), respectively. Pure PbO_2 electrode was prepared with the same experimental conditions in the absence of $Ce(NO_3)_3$.

Characterization.—SEM images of Ce-doped PbO_2 electrodes were obtained from a SUPRA 55VP field emission scanning electron microscope. The operating voltage was 20.0 kV. The energy dispersive X-ray spectroscopy (EDS, Apollo XV, SCHMIDT SCIENTIFIC) was used to examine the composition of Ce-doped PbO_2 electrodes. The structure of Ce-doped PbO_2 electrodes was analyzed by BRUKER X-ray diffraction (XRD). Scherrer's formula was used for the calculation

[z]E-mail: yaoyingwu@hebut.edu.cn; zhaocm_2003@126.com

of crystallite sizes:

$$D = \frac{0.9\lambda}{\beta\cos\theta} \quad [1]$$

where D is the crystallites size, λ is the X-ray wavelength used, β is the broadening of diffraction line measured as half of its maximum intensity and θ is the corresponding angle.

Electrochemical measurements and accelerated life tests.— Electrochemical measurements of Ce-doped PbO_2 electrodes were carried out in a classical three-electrode system which was composed of a Pt sheet as counter electrode and a saturated calomel electrode (SCE) as reference electrode. The PbO_2 electrodes and Ce-doped PbO_2 electrodes (10 mm×10 mm) were used as the working electrodes. The measurement system is CHI 660D electrochemical workstation. Linear sweep voltammetry (LSV) tests were conducted in the potential range of 0–2 V at a scan rate of 1 mV s^{-1} in 0.2 mol L^{-1} Na_2SO_4 solution.

The service lifetime tests of Ce-doped PbO_2 electrodes were investigated in 2 mol L^{-1} H_2SO_4 solution, current density at 4 A cm^{-2} and temperature at 60°C. During the lifetime tests, the cell potential was measured periodically. The lifetime of electrodes can be considered to end when the cell potential steeply increased to higher than 10.0 V.

Electrocatalytic degradation properties.— The oxidation of methylene blue (MB) was carried out in an electrochemical reactor using Ce-doped PbO_2 electrode as anode, stainless steel as cathode and 0.2 mol L^{-1} Na_2SO_4 as supporting electrolyte. The electrolysis conditions were current density at 200 mA cm^{-2}, temperature at 25°C and the electrodes distance with 1 cm. During the experiments, samples were drawn from the reactor at certain intervals and then analyzed. The concentration of methylene blue was determined by measuring the absorbance at a fixed wavelength (665 nm), which corresponded to the maximum absorption wavelength, using INESA L5 UV-visible spectrophotometer (Shanghai, China).

Chemical oxygen demand (COD) was measured by a titrimetric method using dichromate in an acidic solution as the oxidant. The COD removal efficiency (η) was calculated by the following formula:

$$\eta = \frac{COD_0 - COD_t}{COD_0} \times 100\% \quad [2]$$

where COD_0 is the COD of initial concentration and COD_t is the COD at given time t.

Results and Discussion

Electrodeposition process.—Cyclic voltammetry studies.— The cyclic voltammetry curve obtained from lead nitrate solution in the absence of cerium ions was shown in Fig. 1 (curve a). In the anodic branch, the onset potential of lead dioxide electrodeposition (E_{onset}) is at about 1.51 V vs SCE, featured an current growth corresponding to the simultaneous reactions of Pb^{2+} oxidation and oxygen evolution process. In the cathodic branch of the curve, a current peak due to lead dioxide reduction appeared in the potential range of 0.75–1.0 V vs SCE. A hysteresis loop appears in the range of potential from 1.34 V to 1.63 V vs SCE, indicating that lead dioxide nucleation process occurs on the GCE.[24]

Different concentrations of cerium ions (1 and 3 mmol L^{-1}) were added into the lead nitrate solution, the onset potential (E_{onset}) of lead dioxide electrodeposition is positively shifted with the increase of the concentration of cerium ions in the bath, which suggests a remarkable inhibition effect of cerium ions on the lead dioxide electrodeposition. The inhibition can be attributed to the adsorption of cerium ions on the electrode surface, which in the future can form cerium oxide. The formation of cerium oxide inevitably results in the decrease of active sites number on the electrode surface.[23] And the adsorption of cerium ions on the electrode surface also will be followed by the blocking effect.[25] When the cerium ions content surpassed 3 mmol L^{-1} in the solution, the film became rough and unstable during electrodeposition process.

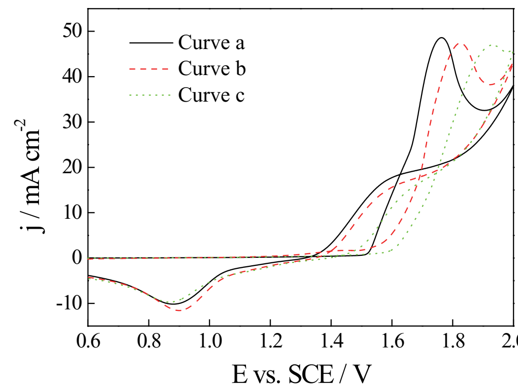

Figure 1. Cyclic voltammograms for the electrodeposition of lead dioxide on GCE at a scan rate of 50 mV s^{-1} in different cerium ions concentrations. (a) 0 mmol L^{-1}; (b) 1 mmol L^{-1}; (c) 3 mmol L^{-1}.

Chronoamperometry study.—Chronoamperometry of lead dioxide electrodeposition on GCE from lead nitrate solution without cerium ions is shown in Fig. 2a. The results show that at first the current density increases and reaches the maximum, then decreases for the nucleation and the growth of new phase. As shown in Table I, the more positive the step potential, the larger the maximum current density (j_m) during the initial stage of lead dioxide electrocrystallization, and the corresponding time (t_m) is less. All the current transients obtained had the feature of a three-dimensional growth nucleation with diffusion control.

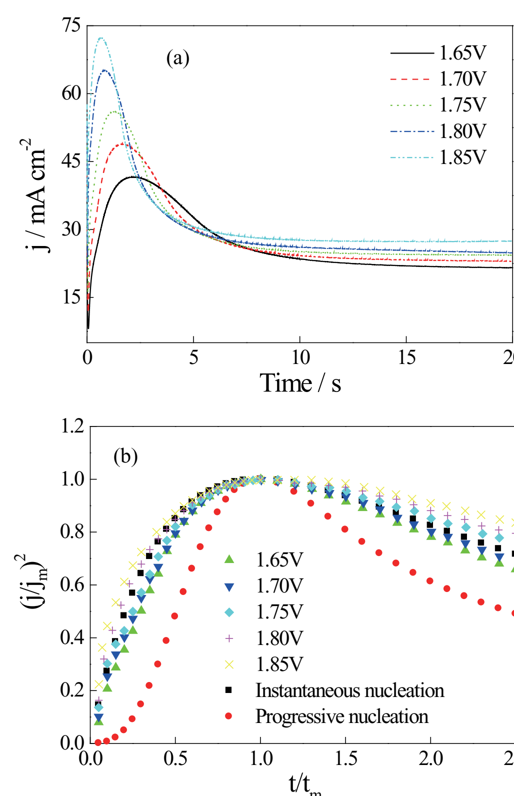

Figure 2. (a) Potentiostatic current transients for lead dioxide electrodeposition on GCE in electrolyte in the absence of cerium ions, (b) Non-dimensional plots of $(j/j_m)^2$ vs. t/t_m for the current transients.

Table I. j_m and t_m of the transient curves for PbO_2 and Ce-doped PbO_2 system with cerium ions (3 mmol L^{-1}).

	PbO_2 system		Ce-doped PbO_2 system with cerium ions (3 mmol L^{-1})	
Potential/ V Vs SCE	t_m/s	j_m/(mA/cm^2)	t_m/s	j_m/(mA/cm^2)
1.65	2.156	41.633	5.181	25.449
1.70	1.651	48.847	2.604	33.003
1.75	1.223	56.005	1.262	49.272
1.80	0.800	65.087	0.850	58.014
1.850	0.640	72.358	0.653	65.851

According to the Scharifker–Hills model,[26] these current transients can be presented in a non-dimensional form by plotting the normalized current $(j/j_m)^2$ vs. time t/t_m. There is a comparison of the theoretical curves through (3) and (4) for instantaneous and progressive nucleation, respectively, with the experimental data, which is used for the determination of the nucleation mechanism. For instantaneous nucleation:

$$\frac{j^2}{{j_m}^2} = \frac{1.9542}{t/t_m}\{1 - \exp[-1.2564(t/t_m)]\}^2 \quad [3]$$

And for progressive nucleation:

$$\frac{j^2}{{j_m}^2} = \frac{1.2254}{t/t_m}\{1 - \exp[-2.3367(t/t_m)^2]\}^2 \quad [4]$$

where j and t are the current density and time, respectively; j_m and t_m are maximums of the current transients.[27]

By using Scharifker–Hills nucleation model, the corresponding data were calculated as shown in Fig. 2b. Clearly, the experiment data were close to the theoretical curve of instantaneous nucleation model. Therefore, it can be concluded that the instantaneous nucleation predominated at all deposition potentials for the electrodeposition process of lead dioxide.

As shown in Fig. 3a, the influence of cerium ions on the nucleation and growth of lead dioxide on GCE from lead nitrate solution was investigated. It can be found that at the same potential, the maximum current density (j_m) of lead dioxide electrodeposition with cerium ions (3 mmol L^{-1}) is smaller than that without cerium ions. With potential moving to the positive direction, the induction time will reduce gradually, the t_m for lead dioxide electrodeposition with cerium ions may be longer than that without cerium ions, which imply that cerium ions can change the conformation of electric double layer on electrode surface. Cerium ions exhibits an obvious inhibition effect on the lead dioxide deposition. It can be observed from Fig. 3b that the nucleation mode of lead dioxide is not changed by cerium ions, and the electrodeposition of lead dioxide is still followed instantaneous nucleation in the presence of cerium ions.

Electrochemical impedance spectroscopy.—The electrochemical impedance spectroscopy (EIS) of lead dioxide on the glass carbon electrode (GCE) from lead nitrate bath in the absence and presence of cerium ions (3 mmol L^{-1}) at 1.7 V vs.SCE is shown in Fig. 4a. From the Nyquist plot, it can be seen that lead dioxide with and without cerium ions composes of a high-frequency capacitive loop followed by a low frequency inductive loop, and the difference between them is that the lead dioxide with cerium ions exhibits bigger radius compared with the lead dioxide without cerium ions. The high-frequency capacitive loop represents the oxidation mechanism in the lead nitrate bath, and it includes the double layer capacitance and the charge transfer resistance. The inductive loop indicates the presence of some adsorbed intermediate.[28] It may be an oxygen-containing intermediate of Pb(III), such as $Pb(OH)^{2+}$, which desorbs from the electrode surface.[23]

The electrochemical equivalent circuit as shown in Fig. 4b including: the solution resistance (R_s) related to solution conductivity, the charge transfer resistance (R_{ct}) linked to the reaction rate and the capacitance of the double layer (C_{dl}). When part of the diagram is located in the negative imaginary part of the plan it means that adsorption/desorption process has occurred and the response exhibits an inductive relaxation.[29] For this, inductance resistance (R_L) and an inductance L are introduced in the equivalent circuit.

It can be calculated that the R_{ct} values of the lead dioxide with cerium ions is 258.1 Ω cm^{-2} which is about 2 times that of the lead dioxide without cerium ions with the R_{ct} of 123.2 Ω cm^{-2}. The difference indicates that the presence of cerium ions slightly modifies lead dioxide deposition kinetic. The C_{dl} value of the lead dioxide with cerium ions (0.389 μF cm^{-2}) is lower than that of the lead dioxide without cerium ions (0.511 μF $cm^{-2)}$. This decrease may be related to the adsorption of cerium ions on the anode, which inhabit the electrodeposition of lead dioxide.

Morphology and structure of Ce-doped PbO_2 electrodes.— The SEM micrographs of pure PbO_2 and Ce-doped PbO_2 electrodes are shown in Fig. 5. There is a remarkable change in the surface morphology of the different electrodes. It can be seen that the morphology of pure PbO_2 electrode displays typical pyramid shape. Compared with pure PbO_2, the grains of Ce-doped PbO_2 electrodes become smaller

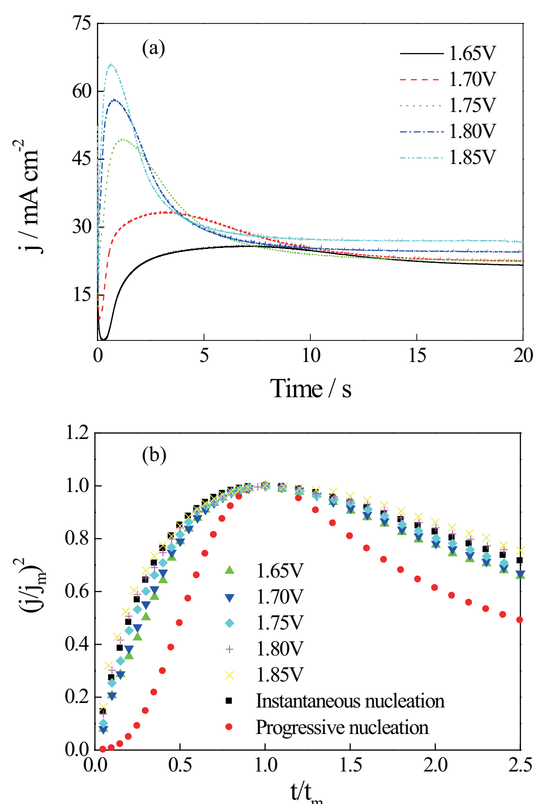

Figure 3. (a) Potentiostatic current transients for lead dioxide electrodeposition on GCE in electrolyte in the presence of cerium ions (3 mmol L^{-1}), (b) Non-dimensional plots of $(j/j_m)^2$ vs. t/t_m for the current transients.

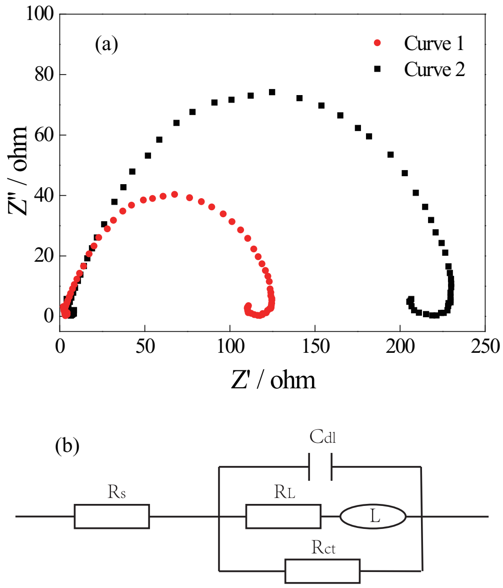

Figure 4. (a) Nyquist plots of lead dioxide on the glass carbon electrode (GCE) from lead nitrate plating bath in the absence (curve 1) and presence (curve 2) of cerium ions (3 mmol L^{-1}) at 1.7 V vs. SCE; (b) Electrochemical equivalent circuits used for fitting the experimental data.

and more compact with the increase of Ce content. The results prove that the adulteration of Ce inhabits the continuous electrodeposition of lead dioxide and decrease grain size. The atomic percentage of cerium in Ce-PbO_2 (1), Ce-PbO_2 (2) and Ce-PbO_2 (3) electrodes is 0.21%, 0.45% and 0.70%, respectively. However, subsequent increase of Ce content make the electrode loose and easily detachment due to excess cerium destroyed the crystallization of PbO_2.[30]

Fig. 6 presents the XRD patterns of PbO_2 and Ce-doped PbO_2 electrodes with different Ce content. It can be seen that pure PbO_2 electrodes were composed of α-PbO_2 and β-PbO_2 phase, and the main diffraction peaks at 25.3°, 32.1° and 49.2° corresponding respectively to (110), (101) and (211) crystal planes of β-PbO_2, and 28.4° corresponding to (111) crystal planes of α-PbO_2. The adulteration of Ce could change their preferred orientation, the α-PbO_2 phase disappear, and the main diffraction peaks are (101) and (301) crystal planes of β-PbO_2. The average grain sizes of PbO_2 electrodes and Ce-doped PbO_2 electrodes are shown in Table II, which were estimated from the half height width of the strongest diffraction peak using the Scherrer equation. The results show that the adulteration of Ce can diminish the crystalline size and the Ce-PbO_2 (3) electrodes had the smallest grain size of 16.2 nm. The result corresponds to the SEM analysis.

Physicochemical properties of Ce-doped PbO_2 electrodes.— Electrochemical property.— Oxygen evolution is a competitive reaction in the electrochemical oxidation process of organic pollutants, which can cause power loss and reduce the current efficiency of organic oxidation. Fig. 7 shows the linear polarization curves of different Ce-doped PbO_2 electrodes in 0.2 mol L^{-1} Na_2SO_4 solution at a scan rate of 1 mV s^{-1}. The results shown that the adulteration of Ce shifts the oxygen evolution overpotential of Ce-doped PbO_2 electrodes more positively. Ce-PbO_2 (3) exhibits the highest overpotential for oxygen evolution, followed by Ce-PbO_2 (2) and then lastly Ce-PbO_2(1). The oxygen evolution potential of the Ce-PbO_2 (1), Ce-PbO_2 (2), and Ce-PbO_2 (3) electrodes are 1.59, 1.71 and 1.77 V vs.SCE at 0.05 A cm^{-2}, respectively, all of which are higher than that of pure PbO_2 electrode, 1.51 V vs.SCE. The results show that the adulteration of Ce can restrain oxygen evolution and promote more oxidizing agent to be used in the degradation of organic pollutants. The higher oxygen evolution overpotential suggested that the electrodes were much more suitable for the degradation of organics than the traditional PbO_2 electrodes.[9,26]

(a)
(b)
(c)
(d)

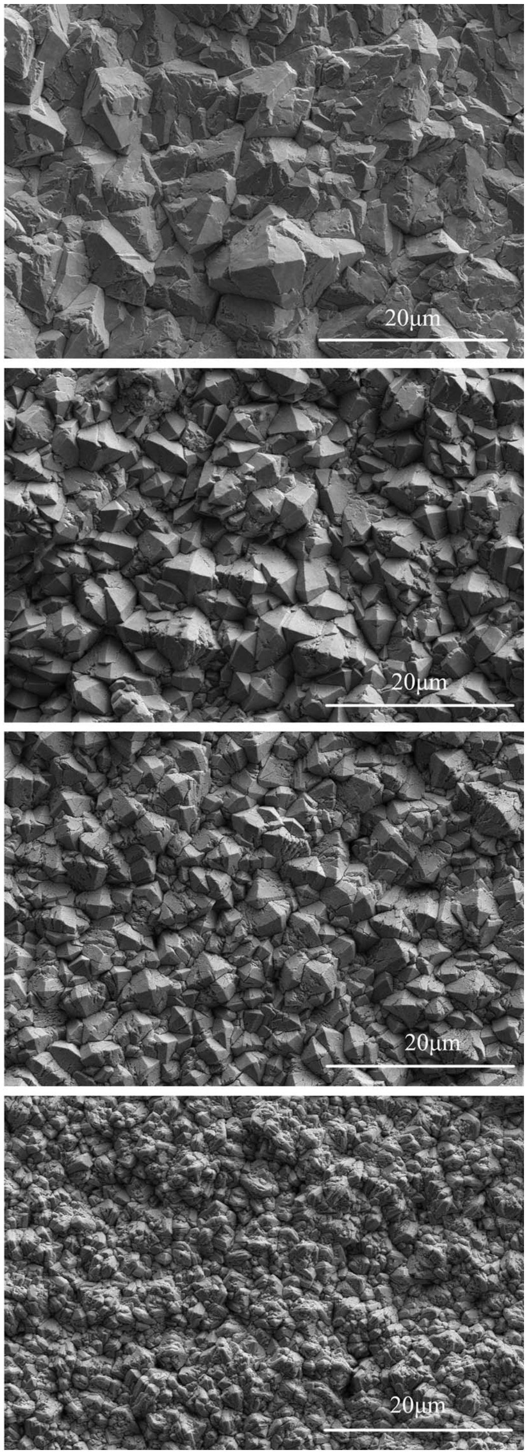

Figure 5. SEM morphology of different Ce-doped PbO_2 electrodes. (a) pure PbO_2; (b) Ce-PbO_2(1); (c) Ce-PbO_2(2); (d) Ce-PbO_2(3).

*Electrode stability.—*Service life is an important factor for practical application of Ce-doped PbO_2 electrode, accelerated life test of different Ce-doped PbO_2 electrodes was carried out and the results were shown in Fig. 8. We can find that the adulteration of Ce can obviously extend the lifetime of the Ce-doped PbO_2 electrode, and the Ce-PbO_2 (3) electrode displays the longest lifetime (74 h), then Ce-PbO_2 (1) (44 h) and Ce-PbO_2 (2) (63 h). The lifetimes of all the aforementioned modified electrodes are far longer than that of PbO_2 electrode, 35 h.

The ionic radius of Ce^{4+} is 87 pm, which is very close to that of Pb^{4+} (77.5 pm). Therefore, during the process of electrodeposition,

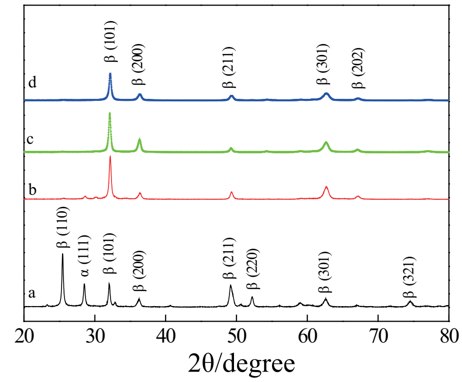

Figure 6. XRD patterns of different Ce-doped PbO_2 electrodes.(a) pure PbO_2; (b) Ce-PbO_2(1); (c) Ce-PbO_2(2); (d) Ce-PbO_2(3).

Table II. Crystal sizes of PbO_2 and Ce-doped PbO_2 electrodes.

PbO_2 electrodes	Crystal sizes (nm)
PbO_2	24.8
Ce-PbO_2 (1)	19.6
Ce-PbO_2 (2)	17.8
Ce-PbO_2 (3)	16.2

it is easy for cerium to form a solid solution with lead oxide via substitution.[31] According to the above results together with SEM and XRD, it is assumed that cerium can diminish the defects of crystals of lead dioxide and make the electrodes more compact. The more compact structure and less defects of the Ce-doped PbO_2 electrodes cannot only effectively hinder the penetration of the electrolyte, but also prevent active oxidative species from diffusing into the Ti substrate,[32] which can also prolong the lifetime of the electrode.

Electrocatalytic property.—Bulk electrolysis was conducted using MB as a model pollutant to explore the electrocatalytic property of different Ce-doped PbO_2 electrodes. Fig. 9a shows MB removal efficiencies of these Ce-doped PbO_2 electrodes. The results show that the MB removal of these Ce-doped PbO_2 electrode during the first 80 min rose linearly and then the removal increases slowly. The MB removal efficiency for all these electrodes is up to 75% within 120 min. The highest removal efficiency was obtained on the Ce-PbO_2 (3) electrode, which was approximately 1.3 times that of pure PbO_2 electrodes. This suggests that the adulteration of Ce can improve the electrochemical activity of PbO_2 electrode for oxidation of organic compounds.

The COD removal efficiencies on the difference Ce-doped PbO_2 electrodes are shown in Fig. 9b. It is clearly observed that COD removal efficiencies on different Ce-doped PbO_2 electrodes increased with time. During 120 min electrolysis, Ce-PbO_2 (3) electrodes exhibited the best COD removal efficiency (70%), and the COD removal efficiency of pure PbO_2 electrodes was the lowest, only reaching 44%. It was worth to notice that COD removal efficiencies were all lower than MB removal efficiencies for different electrodes, indicating that the mineralization of MB was incomplete and some intermediates were produced.[33]

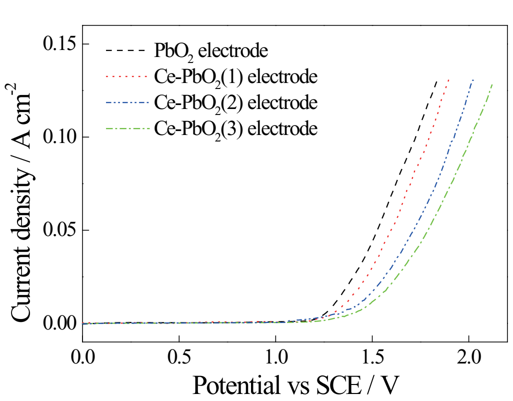

Figure 7. Linear sweep voltammetric curves of different Ce-doped PbO_2 electrodes in 0.2 mol L^{-1} Na_2SO_4 solution.

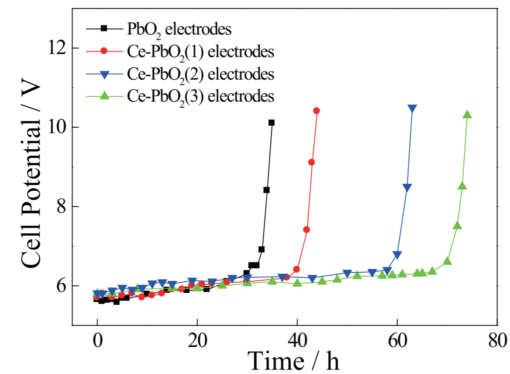

Figure 8. Variation of cell voltage of different Ce-doped PbO_2 electrodes with the time in the accelerated life test.

Conclusions

The influences of cerium ions on the electrodeposition process of lead dioxide from lead nitrate solution was investigated. It is found that E_{onset} is positively shifted with the increase of the cerium ions concentration. Cerium exhibits a remarkable inhibition effect on the lead dioxide electrodeposition. Instantaneous nucleation with three-dimensional diffusion-controlled growth is found for the lead dioxide

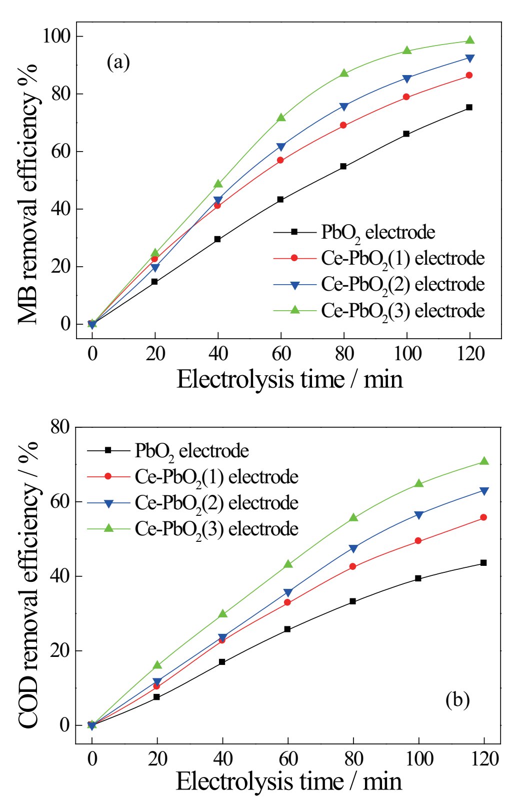

Figure 9. The removal efficiency of MB (a) and COD (b) on the different Ce-doped PbO_2 electrodes.

electrodeposition, which is not influenced in the presence of cerium ions.

The morphology and structure of Ce-doped PbO_2 electrodes was strongly affected by the adulteration of Ce, which can greatly decrease crystalline size. MB degradation experiments showed that electrocatalytic activity of PbO_2 electrodes was greatly improved by the adulteration of Ce. Accelerated life tests indicate that the stability of electrode was greatly enhanced due to the adulteration of Ce, and it will be more preferably used in its practical application.

Acknowledgments

The project was supported by the Natural Science Foundation of Hebei Province of China (B2012202002), the Scientific and Technical Innovation Fund of Hebei University of Technology for Excellent Youth (2011010), the Scientific and Technical Research Fund of Hebei Province for Excellent Youth in University (Y2011104).

References

1. X. H. Li, D. Pletcher, and F. C. Walsh, *Chem. Soc. Rev*, **40**, 3879 (2011).
2. D. Devilliers and E. Mahé, *Electrochim. Acta*, **55**, 8207 (2010).
3. T. Chen, H. Huang, H. Y. Ma, and D. L. Kong, *Electrochim. Acta*, **88**, 79 (2013).
4. F. W. Wang, S. D. Li, M. Xu, Y. Y. Wang, W. Y. Fang, and X. Y. Yan, *J. Electrochem. Soc*, **160**, D53 (2013).
5. M. Hamza, S. Ammar, and R. Abdelhédi, *Electrochim. Acta*, **56**, 3785 (2011).
6. L. S. Andrade, T. T. Tasso, D. L. da Silva, R. C. Rocha-Filho, N. Bocchi, and S. R. Biaggio, *Electrochim. Acta*, **54**, 2024 (2009).
7. M. Panizza and C. A. Martinez-Huitle, *Chemosphere*, **90**, 1455 (2013).
8. S. Abaci, U. Tamer, K. Pekmez, and A. Yildiz, *Electrochim. Acta*, **50**, 3655 (2005).
9. R. Amadelli, L. Samiolo, A. D. Battisti, and A. B. Velichenko, *J. Electrochem. Soc*, **158**, P87 (2011).
10. H. Razmi, H. Heidari, and E. Habibi, *J. Solid. State. Electro*, **12**, 1579 (2008).
11. O. Shmychkova, T. Luk'yanenko, A. Velichenko, L. Meda, and R. Amadelli, *Electrochim. Acta*, **111**, 332 (2013).
12. A. B. Velichenko and D. Devilliers, *J. Fluorine. Chem*, **128**, 269 (2007).
13. Y. Y. Dan, H. Y. Lu, X. L. Liu, H. B. Lin, and J. Z. Zhao, *Int J Hydrogen Energ*, **36**, 1949 (2011).
14. R. Amadelli, L. Samiolo, A. B. Velichenko, V. A. Knysh, T. V. Luk'yanenko, and F. I. Danilov, *Electrochim. Acta*, **54**, 5239 (2009).
15. A. B. Velichenko, R. Amadelli, V. A. Knysh, T. V. Luk'yanenko, and F. I. Danilov, *J. Electroanal. Chem*, **632**, 192 (2009).
16. A. B. Velichenko, V. A. Knysh, T. V. Luk'yanenko, Yu. A. Velichenko, and D. Devilliers, *Mater. Chem. Phys*, **131**, 686 (2012).
17. Y. W. Yao, C. M. Zhao, and J. Zhu, *Electrochim. Acta*, **69**, 146 (2012).
18. Y. Liu, H. L. Liu, J. Ma, and J. J. Li, *J. Hazard. Mater*, **213–214**, 222 (2012).
19. F. W. Wang, X. Y. Yan, M. Xu, S. D. Li, and W. Y. Fang, *Electrochim. Acta* **97**, 253 (2013).
20. X. M. Chen, P. D. Yao, D. H. Wang, and X. Z. Wu, *Chem. Eng. J*, **147**, 412 (2009).
21. Q. Li, Q. Zhang, H. Cui, L. Ding, Z. B. Wei, and J. P. Zhai, *Chem. Eng. J*, **228**, 806 (2013).
22. H. Lin, J. F. Niu, J. L. Xu, Y. Li, and Y. H. Pan, *Electrochim. Acta*, **97**, 167 (2013).
23. O. Shmychkova, T. Luk'yanenko, R. Amadelli, and A. Velichenko, *J. Electroanal. Chem*, **706**, 86 (2013).
24. Z. B. Lin, B. G. Xie, J. S. Chen, J. J. Sun, and G. N. Chen, *J. Electroanal. Chem*, **633**, 207 (2009).
25. S. Y. Ai, M. N. Gao, W. Zhang, Q. J. Wang, Y. F. Xie, and L. T. Jin, *Talanta*, **62**, 445 (2004).
26. B. Scharifker and G. Hills, *Electrochim. Acta*, **28**, 879 (1983).
27. M. Gu, *Electrochim. Acta*, **52**, 4443 (2007).
28. F. Hu and K. C. Chan, *Mater. Chem. Phys.*, **99**, 424 (2006).
29. O. Aaboubi, J. Douglade, X. Abenaqui, R. Boumedmed, and J. Von Hoff, *Electrochim. Acta*, **56**, 7885 (2011).
30. X. Y. Duan, F. Ma, Z. X. Yuan, L. M. Chang, and X. T. Jin, *Electrochim. Acta*, **76**, 333 (2012).
31. Y. Liu, H. L. Liu, J. Ma, and J. J. Li, *Electrochim. Acta*, **56**, 1352 (2011).
32. Y. H. Song, G. Wei, and R. C. Xiong, *Electrochim. Acta*, **52**, 7022 (2007).
33. Y. Wang, Z. Y. Shen, Y. Li, and J. F. Niu, *Chemosphere*, **79**, 987 (2010).